Triaxial projected shell model study of the rapid changes in $B(E2)$ for $^{180-190}$Pt isotopes

G. H. Bhat,[1] J. A. Sheikh,[1,2] Y. Sun,[3,4,2,*] and U. Garg[5]

[1]*Department of Physics, University of Kashmir, Srinagar 190 006, India*

[2]*Department of Physics and Astronomy, University of Tennessee, Knoxville, Tennessee 37996, USA*

[3]*Department of Physics, Shanghai Jiao Tong University, Shanghai 200240, People's Republic of China*

[4]*Institute of Modern Physics, Chinese Academy of Sciences, Lanzhou 730000, People's Republic of China*

[5]*Department of Physics, University of Notre Dame, Notre Dame, Indiana 46556, USA*

(Received 18 July 2012; revised manuscript received 15 September 2012; published 19 October 2012)

The mass region with a proton number just below the magic number $Z = 82$ is known to exhibit a rich variety of shape phenomena. Inspired by the recent extensive experimental measurements of the transition probabilities for the yrast bands in some Pt isotopes in this mass region, we have performed a detailed investigation of $^{180-190}$Pt using the triaxial projected shell model approach (TPSM). It is demonstrated that by performing the exact three-dimensional angular-momentum projection on multi-quasiparticle configurations, constructed from the traxially deformed mean field, the TPSM provides a consistent description of the yrast band structures, the γ-vibrational band, and the second 0^+ band in these nuclei. Further, the observed rapid variations in the quadrupole transition probability along the yrast line of these isotopes are well reproduced in the present study.

DOI: 10.1103/PhysRevC.86.047307 PACS number(s): 21.60.Cs, 21.10.Re, 23.20.Lv, 27.70.+q

The study of nuclear shape changes as a function of particle number, angular momentum, and excitation energy has been one of the important research areas in nuclear structure physics. In particular, in the vicinity of the proton shell closure with $Z = 82$, rapid variations of the nuclear shape have been extensively studied [1]. In the lighter Pb isotopes, one low-lying excited 0^+ state has been observed in all the even-even isotopes from $A = 184$ to 204 [2–4]. In ^{186}Pb [5] and ^{188}Pb [6], two excited 0^+ states have been observed and the hindrance factors for the three α-branches from ^{190}Po and ^{192}Po support the picture where the three-shape minima of prolate, oblate, and spherical coexist within a narrow range of energy. The Hg isotopes also display a broad variety of nuclear shapes [7–12]. In light Hg isotopes, two distinct minima are associated with weakly deformed oblate and well-deformed prolate deformations. For moderate spins, bands coexist with noncollective prolate shapes in some Hg isotopes [13] and at high spins superdeformed states are populated [14,15].

Interesting features of collective motion are known to occur in Pt isotopes as well [16–23]. The coexistence between prolate and oblate shapes has been invoked to interpret the yrast band structures and transition probabilities [16–18] for these isotopes. There has been considerable effort to study nuclear structure properties in Pt isotopes using both heavy-ion [19–22] and Coulomb excitation [23] experiments. Very recently, detailed lifetime measurements of the yrast bands have been performed [24,25] for ^{182,186}Pt isotopes and it has been shown that a steep increase in $B(E2)$ transition probabilities can partially be explained by using the prescription of mixing of two bands corresponding to two different shapes [24]. Detailed theoretical investigation of the ground-state deformations of Pt isotopes from $A = 166$ to 204 has been carried out using the D1S, D1N, and D1M parametrizations of the Gogny energy density functional approach [26]. It is evident from Fig. 1 in Ref. [26] that in the axial limit, a sudden transition from prolate shape to oblate shape is predicted around $A = 188$, in agreement with the results obtained using the Skyrme density functional [27] and the relativistic mean-field approach [28]. However, in a more generalized treatment with broken axial symmetry, also performed in Refs. [26,29], it is evident that potential energy surfaces evolve from prolate shapes in the lighter isotopes with $A = 166$–182 to triaxial shapes or γ-soft for intermediate isotopes with $A = 184$–196 and to oblate shapes for the neutron-rich isotopes. These results are independent of the parametrization employed in the Gogny density functional approach. The theoretical work, therefore, suggests that, from $A = 184$ to 196, Pt isotopes should be studied by using the triaxial mean-field approach. Indeed, the early systematic study of electromagnetic transition properties using the axially symmetric mean field as a starting point indicated a clear deficiency in the wave functions for the description of $^{184-196}$Pt isotopes [30].

The purpose of the present work is to investigate systematically the band structures and transition probabilities of the $^{180-190}$Pt isotopes using the triaxial projected shell model approach (TPSM) [31]. In this model, a three-dimensional angular-momentum projection technique is employed to project out the good angular-momentum states from the triaxially deformed Slater determinant. This approach opens up opportunities to treat problems that otherwise are difficult to interpret in the axial-symmetry limit. For example, the TPSM approach has more recently been used to investigate the interplay between the vibrational and the quasiparticle excitation modes in $^{166-172}$Er [32]. It has been established that low-lying $K = 3$ bands observed in these nuclei are, in fact, built on triaxially deformed two-quasiparticle states. This band is observed to interact with the γ-vibrational band and becomes favored at high angular momentum for some Er nuclei.

Further, it is important to note that $^{180-190}$Pt isotopes have well-developed low-lying γ-vibrational bands that can

*Corresponding author: sunyang@sjtu.edu.cn

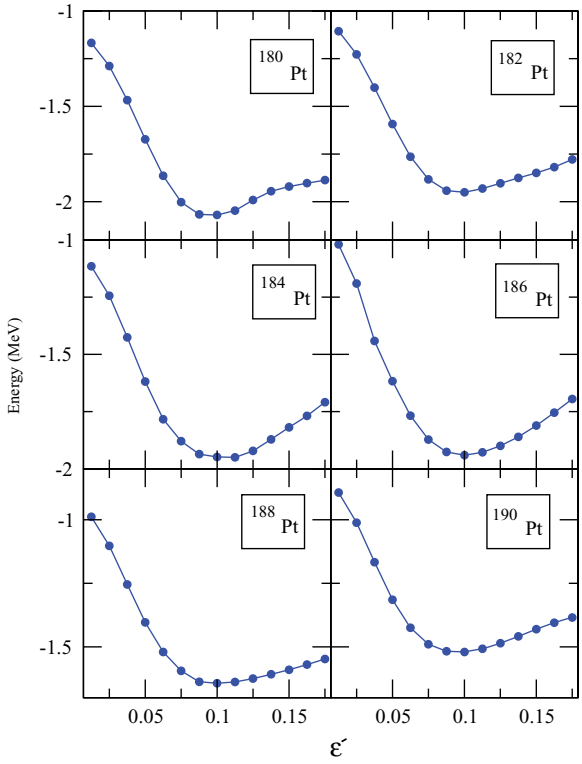

FIG. 1. (Color online) Variation of the projected energy surfaces of the ground state as a function of triaxiality ε' for $^{180-190}$Pt.

be described naturally when triaxial degree of freedom is introduced in the mean field [33]. In the axial-symmetry limit, γ-vibrational bands don't appear in our model and this is the reason that we have also performed a TPSM study of ^{180,182}Pt, as these isotopes have well-developed γ bands.

The TPSM approach has already been discussed in our earlier studies [34–38], and we shall only mention that its basic philosophy is the same as that followed in the standard shell model approach with the only difference being that a deformed basis space is employed rather than a spherical basis shape. The basis is constructed by solving the triaxially deformed mean-field Nilsson Hamiltonian. Such a deformed basis is projected to good angular-momentum states by using the explicit three-dimensional projection technique [39,40]. These projected states are then used to diagonalize the effective shell model Hamiltonian consisting of the pairing plus quadrupole-quadrupole interaction. Although this effective interaction is quite simple as compared to Skyrme density functional, Gogny density functional, or relativistic approaches, it has the advantage that it allows one to perform a systematic analysis of the high-spin band structures of a long series of isotopic chains with a minimal computational effort. Further, in the TPSM study of even-even isotopes, projection is performed from zero-, two-, and four-quasiparticle states and configuration mixing is carried out with such multi-quasiparticle configurations. The later point is known to be crucial in understanding many structural phenomena. In contrast, in most of the "so-called" beyond-mean-field studies using density functional approaches [41–45], projection is restricted to the zero-quasiparticle configuration only.

TABLE I. The axial deformation parameter ε and the triaxial deformation parameter ε' employed in the calculation for $^{180-190}$Pt.

	^{180}Pt	^{182}Pt	^{184}Pt	^{186}Pt	^{188}Pt	^{190}Pt
ε	0.256	0.220	0.218	0.225	0.158	0.128
ε'	0.100	0.100	0.110	0.100	0.095	0.090

In the present work, the Nilsson potential has been solved for the $^{180-190}$Pt isotopes with the deformation parameters listed in Table I. The axial deformation parameters, ε, have been chosen by varying the tabulated values given in Ref. [46] such that the measured value of the $B(E2, 2^+ \rightarrow 0^+)$ transition is described reasonably. This readjustment of the tabulated values is required as the nuclear model employed in the present analysis is different from that used in Ref. [46]. The nonaxial deformations, ε', are chosen in such a way that the bandhead of the γ bands is reproduced. These nonaxial deformations are consistent with the values obtained from the minimum of

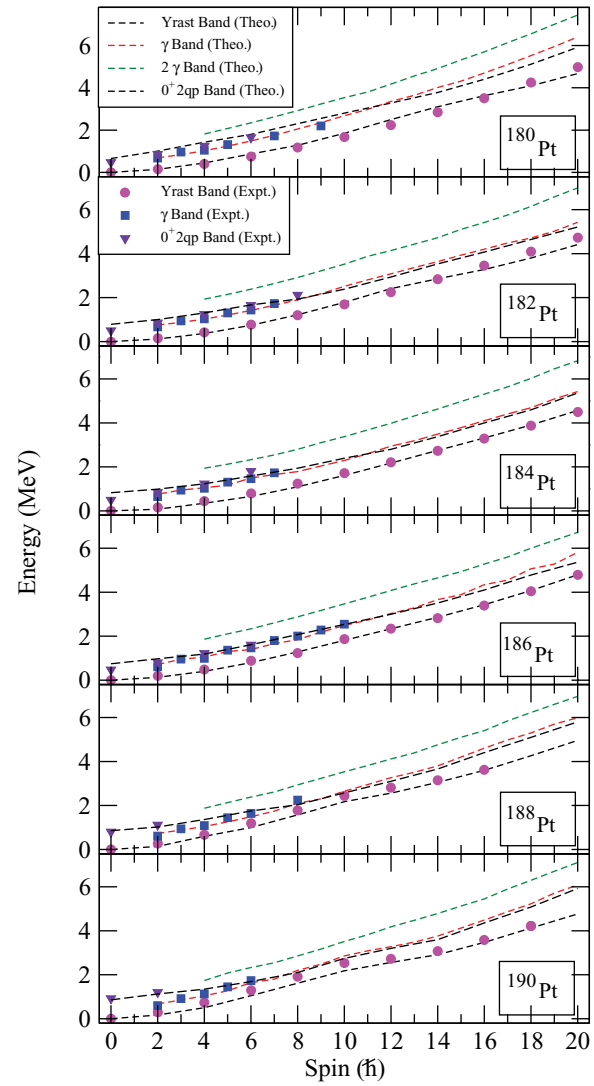

FIG. 2. (Color online) Comparison of the TPSM energies after configuration mixing with the available experimental data for $^{180-190}$Pt. Data are taken from Refs. [47–51].

the potential energy surfaces shown in Fig. 1. In this figure, projected ground-state energy is drawn as a function of the triaxial parameter with the axial deformation parameter being held fixed. It needs to be emphasized that these deformation parameters are used to solve the triaxial potential from which the deformed basis space of the TPSM is constructed. In principle, results of shell-model-type calculations should be independent of the deformation used in constructing the basis. However, in practice, as limited basis space is employed, the final results become dependent on the basis deformation. It is, therefore, important to choose optimum deformations to start with. The pairing interaction parameters employed in the present work are same as those used in our recent work on Er isotopes [32].

In the second stage of the TPSM study, the projected states are then employed as a new basis for diagonalization of the shell model Hamiltonian. In the diagonalization process, the number of projected states employed is nearly 40 for all nuclei studied in the present work. Figure 2 depicts the calculated bands after diagonalization and also displays the corresponding available experimental data. It is important to point out that, although the calculated bands in Fig. 2 are labeled as γ, $\gamma\gamma$, and excited $K = 0^+$ bands, these are only the dominant components in the wave function.

In general, it is quite evident from Fig. 2 that agreement between the TPSM results and the experimental data is quite satisfactory. The crossing of the excited 0^+ band with the γ band is noted to occur at about $I = 8$ for all the Pt isotopes. Unfortunately, only few low-lying states of the excited 0^+ band are experimentally known and it is not possible to corroborate this prediction. For a more detailed comparison of the TPSM results with the experimental data, the level energies of ^{186}Pt are plotted in Fig. 3 as an example. The known experimental levels are well described, and the observed levels of the γ band are also well reproduced.

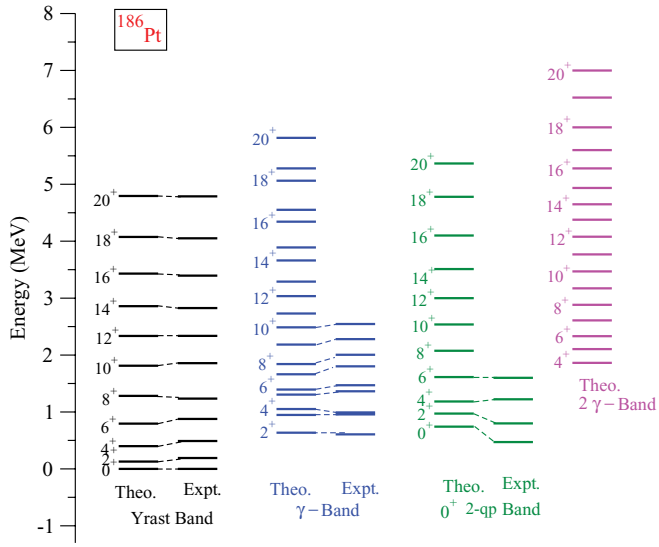

FIG. 3. (Color online) Comparison of the calculated energy levels with the available experimental data for ^{186}Pt. Data are taken from Ref. [49].

The major emphasis of the present work is to elucidate the recent measurement of the lifetimes of the studied Pt isotopes along the yrast line. The data depict a rapid variation of the $B(E2)$ transition probabilities along the yrast band with probabilities showing an increasing trend for low-spin states and a decreasing trend for high-spin states. We have evaluated the transition probabilities of the Pt isotopes using the wave functions of the TPSM analysis. The expressions and other details for the evaluation of transition probability are discussed in our previous works [37,38] and in the present study we present only the results. For $B(E2)$ calculations, standard effective charges, $1.5e$ for protons and $0.5e$ for neutrons, are employed as in our recent work on even-even Er isotopes [32].

In Fig. 4, the calculated $B(E2)$ transition probabilities are compared with the known experimental values. It is quite

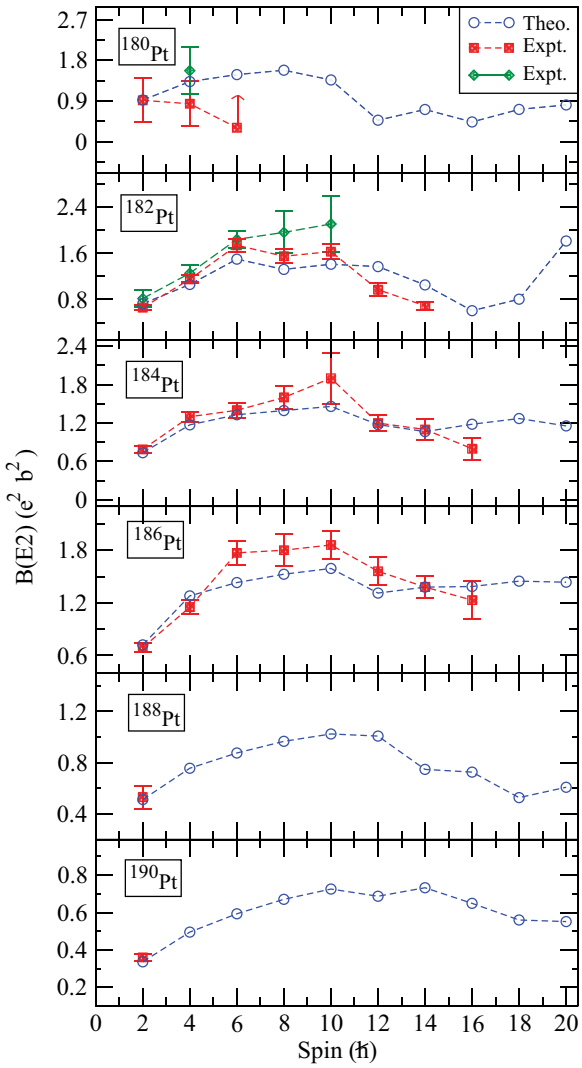

FIG. 4. (Color online) Detailed comparison of the calculated $B(E2)$ values in $^{180-190}$Pt with experimental data [20,24,25,47–51]. There are two sets of experimental data for ^{182}Pt—one from Ref. [24] (shown in red) and the other from Ref. [25] (shown in green). The 4^+ transition in ^{180}Pt (shown in green) is from Ref. [19] and is almost a factor of 2 larger than that given in Ref. [20] (shown in red).

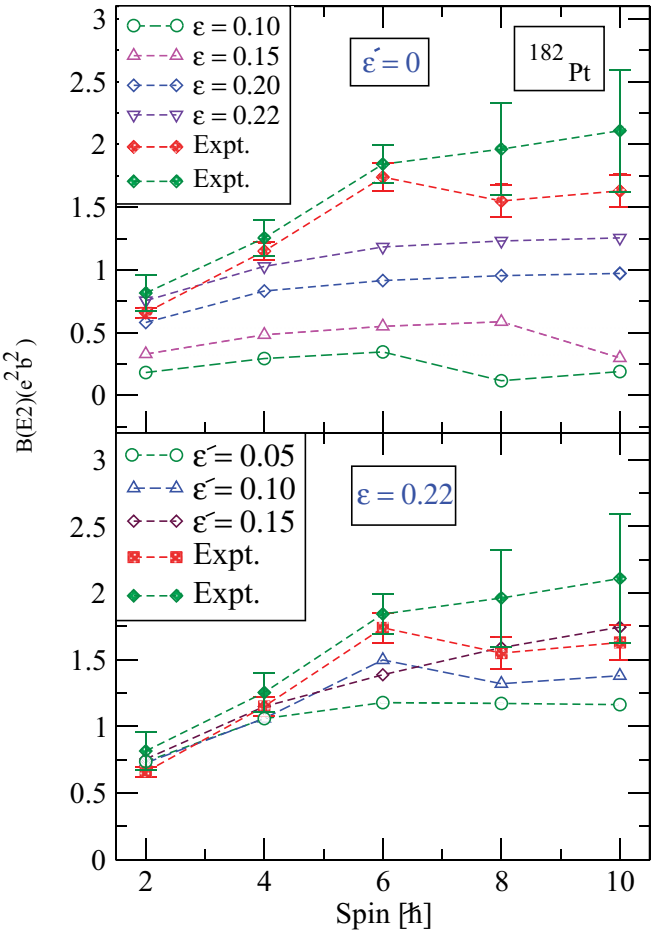

FIG. 5. (Color online) Behavior of the B(E2) values of various configurations as a function of axial and triaxial deformations for ^{182}Pt. In the upper panel, the B(E2) values have been evaluated for a fixed value of $\varepsilon' = 0.0$ and in the lower panel $\varepsilon = 0.22$ has been chosen. There are two sets of experimental data—one from Ref. [24] (shown in red) and the other from Ref. [25] (shown in green).

evident from the figure that the transition probabilities are well reproduced by the TPSM approach. In particular, the increasing trend of $B(E2)$ for low-spin states and the decreasing trend for high-spin states are well described by the calculations. The decreasing trend for high-spin states can be traced to the crossing of the two-quasiparticle neutron configuration with the ground-state band. It is known, in the majority of deformed rare-earth nuclei, that the bands built on high-j unnatural parity orbitals (neutrons in $1i_{13/2}$; protons in $1h_{11/2}$) cross the ground-state band in the spin regime $I = 8$–16. The transition probabilities in the band-crossing region are reduced as these are evaluated between predominantly ground-state and two-quasiparticle aligned configurations.

To understand the mechanism behind the increase of $B(E2)$ for lower spin values, we have calculated transition probabilities with varying ε and ε' and the results are presented in Fig. 5. In the upper panel of the figure, the results are displayed for the axial-symmetry case by taking $\varepsilon' = 0$ and varying ϵ to see the deformation dependence. It is evident from the upper panel that the calculated $B(E2)$ values increase with increasing axial deformation, and the optimum deformation of $\varepsilon = 0.22$ reproduces the first two data points in the $B(E2)$ transition probabilities. However, none of the calculations with an axial deformation only can describe the rapid increase of $B(E2)$ for spin value of $I = 6$. In the lower panel of Fig. 5, calculations for a fixed $\varepsilon = 0.22$ and varying triaxiality ε' are presented. The onset of triaxiality in the deformed basis now increases the $B(E2)$ values for $I = 6$, thus correctly describing the observed variation trend with increasing spin. Therefore, the present calculations provide an alternative to the band-mixing explanation, offered previously, to describe the observed $B(E2)$ behavior.

In summary, in the present work, we have first demonstrated that high-spin band structures of the studied Pt isotopes are reproduced quite well in the TPSM approach. In particular, the yrast bands and the γ bands are described quite satisfactorily. It has been shown that the observed excited 0^+ band has a two-quasiparticle proton structure. The bandhead of this excited band is reasonably well reproduced. Second, we have evaluated the $B(E2)$ transition probabilities along the yrast line that has been the major spotlight of the present investigation. It has been noted that the TPSM approach provides an accurate description of the measured $B(E2)$. In particular, we have shown that both axial deformation and nonaxial deformation contribute to the observed behavior of $B(E2)$ in the low-spin regime. In the high-spin region, it has been substantiated that the drop in the transitions is due to the rotational alignment of neutrons.

One of us (U.G.) thanks colleagues in the Department of Physics for the hospitality extended to him when he visited Shanghai Jiao Tong University (SJTU). Research at SJTU was partially supported by the National Natural Science Foundation of China (Grants No. 11135005 and No. 11075103) and the 973 Program of China (Grant No. 2013CB834401), and research at the University of Notre Dame was supported by the US National Science Foundation (Grant No. PHY-1068192).

[1] K. Heyde and J. L. Wood, Rev. Mod. Phys. **83**, 1467 (2011).
[2] P. Van Duppen, E. Coenen, K. Deneffe, M. Huyse, K. Heyde, and P. Van Isacker, Phys. Rev. Lett. **52**, 1974 (1984).
[3] P. Van Duppen, E. Coenen, K. Deneffe, M. Huyse, and J. L. Wood, Phys. Rev. C **35**, 1861 (1987).
[4] M. Bender, P. Bonche, T. Duguet, and P.-H. Heenen, Phys. Rev. C **69**, 064303 (2004).
[5] A. N. Andreyev *et al.*, Nucl. Phys. A **682**, 482c (2001).
[6] R. D. Page *et al.*, J. Phys. G **25**, 771 (1999).
[7] R. D. Page *et al.*, Phys. Rev. C **84**, 034308 (2011).
[8] J. Elseviers *et al.*, Phys. Rev. C **84**, 034307 (2011).
[9] M. Scheck *et al.*, Phys. Rev. C **81**, 014310 (2010).
[10] M. Scheck *et al.*, Phys. Rev. C **83**, 037303 (2011).
[11] M. Sandzelius *et al.*, Phys. Rev. C **79**, 064315 (2009).
[12] T. Grahn *et al.*, Phys. Rev. C **80**, 014324 (2009).

[13] F. G. Kondev *et al.*, Phys. Rev. C **61**, 011303(R) (1999).
[14] D. Ye *et al.*, Phys. Lett. B **236**, 7 (1990).
[15] R. V. F. Janssens and T. L. Khoo, Annu. Rev. Nucl. Part. Sci. **41**, 321 (1991).
[16] P. M. Davidson, G. D. Dracoulis, T. Kibédi, A. P. Byrne, S. S. Anderssen, A. M. Baxter, B. Fabricius, G. J. Lane, and A. E. Stuchbery, Nucl. Phys. A **657**, 219 (1999).
[17] F. G. Kondev *et al.*, Phys. Rev. C **61**, 044323 (2000).
[18] D. G. Popescu *et al.*, Phys. Rev. C **55**, 1175 (1997).
[19] E. Williams *et al.*, Phys. Rev. C **74**, 024302 (2006).
[20] M. J. A. de Voigt *et al.*, Nucl. Phys. A **507**, 472 (1990).
[21] Y. Oktem *et al.*, Phys. Rev. C **76**, 044315 (2007).
[22] E. A. McCutchan, R. F. Casten, V. Werner, R. Winkler, R. B. Cakirli, G. Gürdal, X. Liang, and E. Williams, Phys. Rev. C **78**, 014320 (2008).
[23] C. Y. Wu *et al.*, Nucl. Phys. A **607**, 178 (1996).
[24] J. C. Walpe, U. Garg, S. Naguleswaran, J. Wei, W. Reviol, I. Ahmad, M. P. Carpenter, and T. L. Khoo, Phys. Rev. C **85**, 057302 (2012).
[25] K. A. Gladnishki, P. Petkova, A. Dewald, C. Fransen, M. Hackstein, J. Jolie, Th. Pissulla, W. Rother, and K. O. Zell, Nucl. Phys. A **877**, 19 (2012).
[26] R. Rodríguez-Guzmán, P. Sarriguren, L. M. Robledo, and J. E. Garcia-Ramos, Phys. Rev. C **81**, 024310 (2010).
[27] P. Sarriguren, R. Rodríguez-Guzmán, and L. M. Robledo, Phys. Rev. C **77**, 064322 (2008).
[28] M. M. Sharma and P. Ring, Phys. Rev. C **46**, 1715 (1992).
[29] T. Nikšić, D. Vretenar, and P. Ring, Prog. Part. Nucl. Phys. **66**, 519 (2011).
[30] B.-A. Bian, Y.-M. Di, G.-L. Long, Y. Sun, J.-Y. Zhang, and J. A. Sheikh, Phys. Rev. C **75**, 014312 (2007).
[31] J. A. Sheikh and K. Hara, Phys. Rev. Lett. **82**, 3968 (1999).
[32] J. A. Sheikh, G. H. Bhat, Y.-X. Liu, F.-Q. Chen, and Y. Sun, Phys. Rev. C **84**, 054314 (2011).
[33] Y. Sun, K. Hara, J. A. Sheikh, J. G. Hirsch, V. Velazquez, and M. Guidry, Phys. Rev. C **61**, 064323 (2000).
[34] J. A. Sheikh, G. H. Bhat, Y. Sun, G. B. Vakil, and R. Palit, Phys. Rev. C **77**, 034313 (2008).
[35] J. A. Sheikh, G. H. Bhat, R. Palit, Z. Naik, and Y. Sun, Nucl. Phys. A **824**, 58 (2009).
[36] J. A. Sheikh, G. H. Bhat, Y. Sun, and R. Palit, Phys. Lett. B **688**, 305 (2010).
[37] J. A. Sheikh, Y. Sun, and R. Palit, Phys. Lett. B **507**, 115 (2001).
[38] G. H. Bhat, J. A. Sheikh, and R. Palit, Phys. Lett. B **707**, 250 (2012).
[39] K. Hara and S. Iwasaki, Nucl. Phys. A **332**, 61 (1979).
[40] K. Hara and S. Iwasaki, Nucl. Phys. A **348**, 200 (1980).
[41] M. Bender and P.-H. Heenen, Phys. Rev. C **78**, 024309 (2008).
[42] T. R. Rodríguez and J. L. Egido, Phys. Rev. C **81**, 064323 (2010).
[43] J. M. Yao, J. Meng, P. Ring, and D. Pena Arteaga, Phys. Rev. C **79**, 044312 (2009).
[44] K. Nomura, T. Otsuka, R. Rodríguez-Guzmán, L. M. Robledo, and P. Sarriguren, Phys. Rev. C **84**, 054316 (2011).
[45] K. Nomura, T. Nikšić, T. Otsuka, N. Shimizu, and D. Vretenar, Phys. Rev. C **84**, 014302 (2011).
[46] P. Möller and J. R. Nix, At. Data Nucl. Data Tables **59**, 185 (1995).
[47] B. Singh and R. B. Firestone, Nucl. Data Sheets **74**, 383 (1995).
[48] C. M. Baglin, Nucl. Data Sheets **111**, 275 (2010).
[49] C. M. Baglin, Nucl. Data Sheets **99**, 1 (2003).
[50] B. Singh, Nucl. Data Sheets **95**, 387 (2002).
[51] B. Singh, Nucl. Data Sheets **61**, 243 (1990).